

1 **Non-stationarity of electrical resistivity and soil moisture**  
2 **relationship in heterogeneous soil system: A case study**

3

4

5 **Michot D.<sup>1\*</sup>, Thomas Z.<sup>1\*</sup>, Adam I.<sup>1,2</sup>**

6

7

8 <sup>1</sup>AGROCAMPUS OUEST, UMR1069, Soil Agro and hydroSystem, F-35000 Rennes, France

9

10 <sup>2</sup> Institut National de la Recherche Agronomique du Niger, Département Gestion des  
11 Ressources Naturelles, BP 429, Niamey, Niger

12

13 Correspondence to: D. Michot ([didier.michot@agrocampus-ouest.fr](mailto:didier.michot@agrocampus-ouest.fr))

14 \*These authors contributed equally to this publication

15

16

1 **Abstract**

2 Understanding the role of vegetation in the interface between the atmosphere and  
3 groundwater is the most decisive key in analyzing the processes involved in water transfer.  
4 The main effect of vegetation is its root water uptake, which significantly modifies the  
5 processes involved in water transfer in the vadose zone. This paper focuses on mapping  
6 temporal and spatial changes in soil moisture using electrical resistivity tomography (ERT).  
7 The main objective is to assess how electrical resistivity (ER) is useful for mapping water  
8 distribution along a heterogeneous toposequence crossed by a hedgerow. Ten ERT were  
9 performed over the studied period for a 28 m long toposequence and compared to matric  
10 potential and groundwater level measurements. Soil Volumetric Water Content (VWC) was  
11 predicted with two methods: (i) from ER using the Waxman and Smits model (ii) and from  
12 matric potential using an experimental retention curve fitted by a Van Genuchten model.  
13 Probability Density Functions (Pdfs) of our set of data show that the largest change, in mean  
14 ER and matric potential, was observed in the topsoil layer. We then analyzed the consistency  
15 between ER and point measurements in this layer by extracting the arrays at the junction of  
16 ER grids and point measurements. Pdfs of ER maps at each monitoring time (from T01 to  
17 T10) were also calculated to select the most contrasting distributions, corresponding to the  
18 wettest (T06) and driest states (T10). Results of ER were consistent with matric potential  
19 measurements, with two different behaviors for locations inside and outside the root zone. A  
20 consistent correlation between VWC values from the Waxman and Smits model and those  
21 obtained from the retention curve was observed outside the root zone. The heterogeneous soil  
22 system inside the root zone shows a different pattern in this relationship. A shift in the  
23 relationship between ER and soil moisture for the locations outside and inside the root zone  
24 highlights the non-stationarity between wet and dry period inside the root zone. The non-  
25 unequivocal of this relationship show the limitation of using ER to predict soil moisture in  
26 heterogeneous soil system. Such systems were actually related to the high hedgerow root  
27 density and also to a particular topographical context (ditch and bank) that is encountered in  
28 Brittany and throughout northwestern Europe.

29

30 Key words: Electrical resistivity tomograph, soil moisture, rhizosphere, matric potential, root  
31 system, heterogeneous soil

32

## 1 **1 Introduction**

2 Understanding the role of vegetation in the interface between the atmosphere and  
3 groundwater is the most decisive key for analyzing the processes involved in water transfer.  
4 The main impact of vegetation is root water uptake and hydraulic redistribution, which  
5 significantly modifies the processes involved in water transfer in the vadose zone. In Western  
6 Europe, hedgerow networks are a common and ancient tree alignment surrounding  
7 agricultural fields. Hedgerow removal due to farm enlargement is the major land use change  
8 since the Second World War. Previous studies suggest a significant impact of hedgerows on  
9 soil moisture (Caubel, 2001; Thomas et al., 2008) and rainfall distribution (Ghazavi et al.,  
10 2008). Many studies have explored the effect of hedgerows surrounding wetlands on water  
11 fluxes and the subsequent increase in transpiration (Thomas et al., 2012) and decrease in  
12 nitrate concentration (Grimaldi et al., 2009). The benefits of hedgerows in soil conservation  
13 have been highlighted by Walter et al. (2003). In agricultural landscapes throughout the  
14 world, combining trees and crops seems an appropriate alternative for providing the benefits  
15 of trees to crop requirements. Water availability can be monitored using direct and indirect  
16 soil moisture sensors. As significant spatial variability exists in the vadose zone, a dense array  
17 of sensors (e.g. tensiometers, TDR, piezometers) is usually required. However, a high density  
18 of sensors is not only expensive, but drilling to install them can disrupt hydraulic contact and  
19 induce preferential flow. Non-invasive geophysical imaging techniques, such as electrical  
20 resistivity tomography (ERT), might be an alternative way to monitor matric-potential  
21 distribution in the soil in relation to root water uptake. Specifically, ERT allows the spatial  
22 distribution of soil electrical resistivity (ER) to be mapped in 2D or 3D.

23 As a geophysical signal, ER is related to varying physical and chemical characteristics. ERT  
24 helps to identify spatial and temporal soil physical properties (e.g. structure, water content,  
25 fluid composition). Many applications of ERT have been developed over the last 20 years,  
26 from assessment of solute transport in aquifers (Muller et al., 2010) to detection of soil  
27 salinity in irrigated zones (Adam et al., 2012). Samouëlian et al. (2005) reviewed ER as a  
28 function of soil properties, described the main electrical devices for 2D or 3D surveys and  
29 explained the basic principles of data interpretation. Soil ER mainly involves the constant  
30 physical properties of the soil, such as clay content, but also involves variable properties over  
31 time, such as soil water content, soil water electrical conductivity and temperature (Ward,  
32 1990; Samouëlian et al., 2005). Thus, time-lapse ERT is an alternative way to monitor spatial  
33 and temporal water flux providing larger spatial scales. Numerous studies have tested the

1 potential of ERT to monitor water flux processes, such as infiltration in unsaturated  
2 conditions (Descloitres et al., 2008; Al Hagrey and Michaelsen., 1999; Michot et al., 2001;  
3 Michot et al., 2003; Yamakawa et al., 2011; Zhou et al., 2001). Thus, in order to use ER to  
4 monitor VWC, it is necessary to perform a laboratory or field calibration (Michot, 2003), or to  
5 develop a pedotransfer function integrating data about soil properties (Hadzick et al., 2011;  
6 Brillante et al., 2014). Another alternative is to use a petro-physical model linking ER to  
7 VWC. Various petro-physical models have been derived from Archie's (1942) law and were  
8 developed first for pure sand (without any clay). The empirical Waxman and Smits (1968)  
9 model based on Archie's (1942) law takes into account the effect of clays on resistivity and  
10 has been successfully applied in its simplified form to agricultural soils (Garré et al., 2011;  
11 Beff et al., 2013). Among five petro-physical models tested on a loamy soil to predict VWC  
12 and soil bulk density, the Waxman and Smits model appeared more consistent for electrical  
13 resistivity values  $> 100\Omega\text{m}$  (Laloy et al., 2011), which are often observed in dry soils. For  
14 lower ER values ( $<100\Omega\text{m}$ ), the volume-averaging method (Pride, 1994; Linde et al., 2006)  
15 outperformed other tested models. A review of possible techniques to develop models that  
16 allow the use of ERT to spatialize soil water availability to plants was presented by Brillante  
17 et al. (2015). They describe methods and models to calibrate ER using TDR measurements.  
18 Several authors have also described the distribution and biomass of tree roots using ERT  
19 (Amato et al., 2008; Amato et al., 2009; Zenone et al., 2008; Al Hagrey and Petersen, 2001;  
20 Rossi et al., 2011). Root presence in the soil is characterized by a highly resistive area close to  
21 the tree trunk (Amato et al., 2008; Al Hagrey, 2007), and soil ER varies with root biomass  
22 density (Rossi et al., 2011). However, understanding the spatial heterogeneity of soil water  
23 content and the hydrological processes in a hedgerow landscape implies estimating the root  
24 water uptake of tree hedgerows. Werban et al. (2008) used ERT to monitor temporal changes  
25 in the distribution of soil water content in the root zone of a lupine plant in the laboratory.  
26 Garré et al. (2011) used ERT to measure soil water depletion caused by barley plants grown  
27 on an undisturbed soil monolith in a lysimeter. Michot et al. (2003) monitored soil water  
28 fluxes with ER imaging in an agricultural field after irrigation and detected preferential  
29 dryness just below cultivated maize plants. Similar observations of root zone drying,  
30 highlighted by an increase in ER, were shown in Mediterranean contexts by Al Hagrey (2007)  
31 and Nijland et al. (2010) on soils planted with cork oaks or covered by semi-natural  
32 vegetation of evergreen shrubs and trees. However, only Srayeddin and Doussan (2009) have  
33 quantified and mapped root water uptake of maize and sorghum in field conditions using

1 time-lapse ERT. Recently, Garré et al. (2012) tested the ability of different ERT electrode  
2 arrays to detect soil moisture dynamics in a monocropping and an intercropping system. The  
3 most promising electrode array they tested was a combination of dipole-dipole and Wenner  
4 measurements. This effective electrode array was then tested for monitoring soil water  
5 dynamics in mixed cropping systems in the warm and humid tropical climate of Thailand  
6 (Garré et al., 2013). Most previous ERT work on soil water depletion induced by tree or plant  
7 root water uptake has focused on well-drained soils.

8 The present study had a double goal: (i) to investigate effects of hedgerow roots on soil  
9 moisture using ERT and point monitoring and (ii) to verify the correlation between ER and  
10 soil moisture in a heterogeneous soil system. Soil water depletion was estimated by point  
11 measurements of soil matric potential over the studied period. ER values were converted to  
12 soil volumetric water content (VWC) using the Waxman and Smits petro-physical model.  
13 VWC values were compared to those obtained from matric potential using a retention curve.  
14 Our case study focused on a toposequence located in a hillslope whose hydrology was  
15 controlled by shallow groundwater. The toposequence was located in a bottomland crossed by  
16 a hedgerow. The hydrological year was particularly wet.

## 17 **2 Materials and methods**

### 18 **2.1 Study site**

19 The study site was located in Brittany, western France. Hillslope hydrology was controlled by  
20 shallow groundwater developed in schist bedrock with silt loam soils. An oak hedgerow  
21 (*Quercus robur*) running north-to-south, planted perpendicular to the slope, created a clear  
22 barrier between two contrasting zones. Upslope of the hedgerow, the only land use was well-  
23 drained hillslope soils with permanent pasture. Downslope of the hedgerow was a bottomland  
24 with waterlogged soils and both permanent pasture and wet-meadow vegetation (*Carex* spp.).  
25 A 28-m toposequence perpendicular to the hedgerow was established from 16 m upslope of  
26 the hedgerow (UP16) to 12 m downslope (DW12). The mean slope was 4.8% and 11.8%,  
27 respectively, on the toposequence upslope and downslope of the hedgerow. The difference in  
28 elevation between UP16 and DW12 was about 2 m (Fig. 1). In the study site, the wetland  
29 extended from 10 m downslope the hedgerow to the stream.

30 Long-term (32-year mean) annual rainfall (R) at a nearby weather station (Le Rheu, 5 km  
31 from the study site) was ~720 mm, annual potential evapotranspiration (PET-Penmann) was

1 ~650 mm, and annual air temperature was ~11.7°C, ranging from 5.4°C in January to 18.4°C  
2 in August (Ferren, 2004). During the studied period, rainfall and PET data were collected at  
3 the Saint-Jacques meteorological station (48° 4' 12" N, 1° 43' 36" W), 5 km from the study  
4 site. Ten monitoring times from 10 March to 13 August 2007 are denoted T01 to T10.  
5 Cumulative rainfall and PET-Penmann were calculated between each monitoring time (T01 to  
6 T10) (Fig. 2a). Annual net rainfall (rainfall – PET) of 7 years (from 2000 to 2007), highlights  
7 that the hydrological year studied was particularly wet (Fig. 2b). During the monitoring  
8 period, net rainfall (Rainfall–PET) of each interval between ERTs was higher than that during  
9 the same period of the previous 6 years (2001-2006) (Fig. S1). Also, the lowest net rainfall  
10 measured between ERTs during the monitoring period was about -40 mm, compared to -150  
11 mm observed during the previous 6 years. Thus, the hydrological year studied was  
12 particularly wet.

## 13 **2.2 Soil organization and properties**

14 The organization and geometry of soil horizons was described in 2D vertical cross section of  
15 the toposequence in a trench of 2 m deep and 28 m long that was excavated parallel to the  
16 toposequence (Fig. 1). Soils and horizons were identified according to the World Reference  
17 Base of Soil Resources (FAO, 2006).

18 The geometry and properties of these pedological horizons vary greatly over small spatial  
19 scales, according to previous observations in a similar hedged landscape (Walter et al., 2003;  
20 Follain et al., 2009). We observed a luvic and stagnic Cambisol and a stagnic Fluvisol from  
21 upslope to downslope, respectively. In the upslope zone, the thickness of the organo-mineral  
22 loamy A horizon increased from 0.4 m to 1.1 m from upslope to the ditch close to the  
23 hedgerow (Fig. 1). In the downslope zone, the organo-mineral A horizon was thinner and  
24 ranged from 0.1 m below the hedgerow to 0.5 m at the boundary with the epistagnic fluvic  
25 horizon (B1 horizon, see Fig. 1) of the wetland. The complexity of this soil's spatial  
26 organization within the hedged landscape is controlled by past and recent redistribution  
27 processes, such as hydric and tillage erosion. Also, past and recent hedgerow network design  
28 may influence soil organization, as highlighted by Follain et al. (2009). Increasing thickness  
29 of the A horizon from upslope to the hedge is due to the anti-erosive effect of the hedge as a  
30 barrier. Soil horizon organization differed slightly below the hedgerow, particularly due to  
31 anthropogenic topographical features, such as under the ditch and in the soil bank (Fig. 1).  
32 Soil thickness above the weathered schist bedrock varied greatly. It ranged from 1.3-1.6 m

1 near the hedgerow in the upslope zone to less than 0.9 m in the downslope zone.  
2 Redoximorphic features appeared below a depth of 0.5 m in the upslope zone and began at the  
3 soil surface in the downslope zone.

4 Soil texture, bulk density and hydraulic conductivity were measured at seven locations along  
5 the toposequence (Fig. 1) where soil matric potential ( $\Psi$ ) and groundwater level (GWL) were  
6 monitored: 16 m, 8 m, 4 m and 1 m upslope (UP16, UP8, UP4 and UP1) and 2 m, 6 m, 12 m  
7 downslope (DW2, DW6 and DW12).

8 The clay content of shallow and organo-mineral horizons ranged from 14.6-16.0% in the  
9 upslope zone and exceeded 20% in the downslope zone (Ghazavi et al., 2008). At greater  
10 depths, the endostagnic B horizon observed in the luvisol Cambisol (UP16) had a clay content  
11 of 23.3%, but the highest clay content was observed in the stagnic Fluvisol in the bottomland  
12 (DW12). It ranged from 24.7% in the shallow epistagnic fluvic B1 horizon to 27.1% in the  
13 endostagnic fluvic B2 horizon at depths of 0.4 m to 0.9 m. At depth, the schist saprolite (C  
14 mineral horizon) had a loam-sandy-clayey texture (Table I in Ghazavi et al., 2008). We  
15 observed several coarse particle accumulations (e.g. stones, quartz veins) in the 2D vertical  
16 soil cross section, in particular in the upslope zone and near the ditch along the hedgerow.

17 As expected, soil bulk density increased with soil depth at all distances along the  
18 toposequence (Fig. S2 a and b, in the Supplement). Vertically, variability in bulk density in  
19 the upslope zone was lower than that in the downslope zone. Horizontally, in the upslope  
20 zone, soil bulk density increased with distance from the hedgerow, respectively, from 1.3  
21 (UP4) to 1.6 (UP16) at 5 cm deep and from 1.5 (UP4) to 1.7 (UP16) at 100 cm deep (Fig. S1  
22 a and b, in the Supplement). Additionally, bulk density was higher in the topsoil layer (0-50  
23 cm deep) in the upslope versus downslope zone.

24 Soil hydraulic conductivity was measured at conditions of near saturation, i.e. at a low water  
25 potential of -0.05 kPa, with a Decagon 4.5-cm diameter mini disk infiltrometer (Decagon  
26 Devices, 2006). Soil hydraulic conductivity was determined from steady-state flux data  
27 according to the Wooding (1968) approach. Multiple depths were measured at each monitored  
28 location along the toposequence (Fig. S2 c and d, in the Supplement). As a function of  
29 changes in bulk density, hydraulic conductivity at -0.5 hPa water potential ( $K_{(-0.5 \text{ hPa})}$ )  
30 decreased with increasing soil depth at all locations along the toposequence except for DW2,  
31 where a singular point was observed at a depth of 60 cm. Mean  $K_{(-0.5 \text{ hPa})}$  values were  
32 significantly higher in the downslope zone ( $6 \cdot 10^{-4}$ ,  $5.7 \cdot 10^{-4}$  and  $5.5 \cdot 10^{-4} \text{ m}\cdot\text{s}^{-1}$  at DW2, DW6

1 and DW12, respectively) versus the upslope zone, especially in the topsoil i.e. depth >50 cm  
2 ( $200 \cdot 10^{-6} \text{ m} \cdot \text{s}^{-1}$  at UP4, UP8 and UP16).  $K_{(-0.5 \text{ hPa})}$  values (Figs. S2c and d, in the Supplement)  
3 were relatively homogeneous in the vertical plane upslope from the hedgerow; while a  
4 difference of two orders of magnitude was observed between the topsoil and subsoil in the  
5 downslope zone. A lower K and higher bulk density are well-known characteristics of  
6 bottomland soils.

7 The soil surface occupied by roots along the trench was estimated using a quadrat of  $1 \text{ m}^2$   
8 subdivided into 100 squares of  $100 \text{ cm}^2$  each (Breda et al., 1995). First, the quadrat was  
9 located at a depth of 10-110 cm to avoid counting pasture roots in the top layer. Otherwise,  
10 roots without woody structure were not considered. For each  $100 \text{ cm}^2$  square, only the woody  
11 roots were counted and summed for the  $1 \text{ m}^2$  section of the trench, both upslope and  
12 downslope, and the percentage of total woody roots that occurred in each section was  
13 calculated as presented by Ghazavi et al. (2008). Along the toposequence, vertical root  
14 distribution within each 1 m was also calculated at four depth classes: 10-50, 50-100, 100-  
15 150, and 150-200 cm (Figs. S2 e and f, in the Supplement). According to the observations of  
16 Ghazavi et al. (2008), horizontal distribution of tree roots in the upslope and downslope zones  
17 was asymmetric, with 76% of tree roots located upslope and only 24% of roots located  
18 downslope. Vertically, tree roots reached deeper in the upslope zone than in the downslope  
19 zone. Moreover, in the upslope zone, 61%, 36%, 3% of roots were, respectively, located 10-  
20 50, 50-100, and 100-200 cm deep. In the downslope zone, 92% of roots were located 10-50  
21 cm deep, and only 8% were 50-100 cm deep.

### 22 **2.3 Hydrological monitoring: point measurements**

23 Soil matric potential and groundwater level were monitored as described by Ghazavi et al.  
24 (2008, 2011). Seven locations were monitored continuously with one piezometer and five  
25 tensiometers each (Fig. 1). Three piezometers were located at 16, 8 and 4 m upslope of the  
26 hedgerow, each with a tube diameter of 11.2 cm and a total length of 7.5 m, of which 4 m at  
27 its base were screened. The other four piezometers were located at 1 m upslope and 2, 6 and  
28 12 m downslope of the hedgerow, each with a diameter of 6.8 cm and a total length of 4.5 m,  
29 of which 2 m at its base were screened. For each monitored location, five tensiometers were  
30 installed at depths of 25, 50, 100, 150, and 200 cm. The vertical soil matric-potential profiles  
31 were used to interpret the ER.



## 1 2.4 Electrical resistivity monitoring

### 2 2.4.1 Timeframe ERT

3 Temporal monitoring of ER along the toposequence (Fig. 1) was performed at 10 monitoring  
4 times (T01 to T10). Resistivity was measured with a Syscal R1 resistivity meter (Iris  
5 Instruments, Orléans, France). The precision of its intensity and voltage was  $\pm 0.3\%$  which is  
6 consistent with measurements taken under constant surface conditions. The experimental  
7 design included a row of 64 electrodes that were lined up on the soil surface perpendicular to  
8 the hedgerow (Fig. 1). With an electrode spacing of 0.5 m, the experimental device measured  
9 31.5 m long. The electrodes remained on the soil surface during the entire experiment to  
10 avoid changes in electrode polarization and ensure high-quality measurements. The  
11 resistivimeter followed a pre-programmed measurement sequence, and a multiplexer switched  
12 among the electrodes.

13 A dipole-dipole arrangement was chosen because it allowed the greatest number of  
14 measurements for the number of electrodes present, which was advantageous for data  
15 inversion. Moreover, the dipole-dipole array was highly sensitive to horizontal changes in  
16 resistivity but relatively insensitive to vertical changes. For each resistivity measurement, an  
17 electrical current was passed between two adjacent electrodes (dipole AB), and the potential  
18 difference was measured between two other neighboring electrodes (dipole MN). The bulk  
19 ER  $\rho_a$  of a half-space measured with a dipole-dipole electrode array is:

$$20 \quad \rho_a = 2\pi \frac{\Delta V}{I} \frac{1}{(1/MA - 1/MB + 1/NB - 1/NA)} = k \frac{\Delta V}{I} \quad (1)$$

21 Where  $I$  is the intensity of the current passed between electrodes A and B,  $\Delta V$  is the potential  
22 difference measured between electrodes M and N, and  $k$  is the “geometric factor”, whose  
23 value depends on the type of array. For a dipole-dipole array,  $k$  is calculated as:

$$24 \quad k = \pi(n \cdot (n + 1) \cdot (n + 2) \cdot a) \quad (2)$$

25 Where  $a$  is the spacing (distance, in m) between electrodes of each dipole, and  $n$  is a dipole-  
26 separation factor whose value is usually an integer multiple of the distance between the  
27 current or potential electrode pair. To obtain the necessary resolution, 646 measurements were  
28 taken during each ERT. Measurements were located at 12 pseudodepths of investigation, the  
29 first 5 with  $a$  of 0.5 m and  $n$  of 1, 2, 3, 4 and 6. Since the potential measured between M and

1 N decreases rapidly with increasing  $n$ , it is not advisable for  $n$  to exceed 6. To maintain  
2 measurement quality at greater depths, which have high signal-to-noise ratios, three  
3 pseudodepths were investigated with  $a$  of 1 m and  $n$  of 2, 3 and 4. The remaining four  
4 pseudodepths had  $a$  of 1.5 m and  $n$  of 2, 3, 4 and 5. In a dipole-dipole electrode setup, the  
5 spacing between the dipole that passes the current and the dipole that measures the potential  
6 difference is gradually increased. By convention, bulk ER measurements are represented at  
7 the centre of the quadripole and at a depth proportional to the spacing between dipoles. Each  
8 ERT required 1 hour and 40 minutes.

#### 9 2.4.2 ERT data processing

10 Inverting resistivity measurements is an essential step before interpreting them because the  
11 raw resistivity measurements rarely reveal the true structure of the soil. Thus, resistivity  
12 sections were inverted with the software RES2DINV (Loke and Barker, 1996) using a  
13 smoothness-constrained least-square method to produce a 2D subsurface model. In the first  
14 iteration, a homogeneous earth model was used as a starting point from which partial  
15 derivative values of resistivity could be calculated analytically. For subsequent iterations, a  
16 quasi-Newton method was used to estimate the partial derivatives, which reduced computing  
17 time. In this method, Jacobian matrices for the homogeneous earth model were used for the  
18 first iteration, and those of subsequent iterations were estimated with an updating technique.  
19 The model consisted of a rectangular grid. Software determined the resistivity of each mesh,  
20 which calculated the ER of each section according to field measurements. An iterative  
21 optimization method consisted of minimizing the difference between measured resistivity  
22 values and those calculated with the inversion model by minimizing the root mean square  
23 error (RMSE). Topographic correction was applied to this inversion process. The cells of the  
24 grid obtained (Fig. S3, in the Supplement) were defined by their 4 corners coordinates. Each  
25 ERT was inverted independently, considering the same number of measurements. Further  
26 details about inversion methods are available in the literature (Loke and Barker, 1996).

27 Bulk ER of unsaturated soils decreases when water content increase, and vice versa (Ward,  
28 1990). In saturated zones, changes in bulk ER are usually linked to changes in groundwater  
29 electrical conductivity.

30 During the monitoring period, soil drying due to evapotranspiration was analyzed using  
31 statistics of each ER map. A probability density function (Pdf) of the map at each monitoring  
32 time (T01 to T10) was calculated, and Pdfs were compared to select the most contrasting

1 distributions. The lowest ER mean represents the wettest state (T06), while the highest ER  
2 mean represents the driest state (T10). The change in ER was calculated between those states  
3 and was compared to that in matric potential for the same states.

#### 4 2.4.3 ER conversion to VWC

5 To quantify the relationship between ER and matric potential, ERs values were extracted at  
6 the location of each tensiometer (Fig. S3, in the Supplement). ER and matric potential of the  
7 topsoil layer (at depths of 25 and 50 cm) corresponding to the unsaturated zone were  
8 analyzed. ER values were also converted to soil VWC from the Waxman and Smits (WS)  
9 model (Waxman and Smits, 1968) simplified by Garré et al. (2011, 2013) using equation (3).

$$10 \quad SWC = \left\{ \frac{\left[ \frac{1}{ER} - b \right]}{a} \right\}^{1/n} \quad (3)$$

11 where  $a$  ( $S \text{ m}^{-1}$ ),  $b$  ( $S \text{ m}^{-1}$ ), and  $n$  are fitting parameters. As explained by Garré et al. (2011),  
12 these parameters can be explained in a physical way in combination with porosity:  $a$  is related  
13 to pore water conductivity, and  $b$  is related to soil surface conductivity. The parameter  $n$  is  
14 related to pore connectivity in the full WS model.

15 Since the variation range of WS parameters is unknown for the toposequence studied, a  
16 sensitivity analysis was performed using the range of the parameters presented by Garré et al.  
17 (2011). Their study examined four horizons of an orthic Luvisol developed in a Loess parent  
18 material from Germany. Orthic Luvisol has relatively similar pedogenesis and texture as those  
19 observed in our toposequence, especially in the upslope zone. For each parameter of the WS  
20 model, three values (Table 1) were tested, leading to 27 simulations. VWC values were  
21 calculated for each extracted cell grid.

22 Using the retention curves from Ghazavi et al. (2011), measured in the soil horizons of this  
23 studied toposequence, we also converted soil matric potential data into VWC. Experimental  
24 retention curves (Fig. S4, in the supplement) were fitted using the Van Genuchten model (Van  
25 Genuchten, 1980) from equation (4):

$$26 \quad \theta(h) = \begin{cases} \theta_r + \frac{[\theta_s - \theta_r]}{[1 + |\alpha \cdot h|^n]^m} & \text{for } h < 0 \\ \theta_s & \text{for } h \geq 0 \end{cases} \quad (4)$$

27 where  $\theta_s$  and  $\theta_r$  are saturated and residual volumetric water content (VWC [ $\text{cm}^3 \text{cm}^{-3}$ ]),  
28 respectively;  $h$  is pressure head or matric potential [hPa]; and  $\alpha$ ,  $n$  and  $l$  are Van Genuchten  
29 parameters  $m=1-l/n$  (Table S1, in the supplement).

## 1    **3    RESULTS**

### 2    **3.1    ER sections and statistical distribution of ER**

3    Pdfs of ER at each measurement time (from T01 to T10) were Gaussian and similar to each  
4    other except at T10 (Fig. 3). T06 and T10 had the greatest differences in ER value statistics  
5    (see Table 1) and were selected as the wet and dry states, respectively. To avoid redundancy,  
6    we describe only ER maps of T06 and T10. The 10 measurement dates (from T01 to T10) are  
7    in the supplements (Fig. S5). At both dates, a superficial layer from 0-0.8 m deep in the  
8    upslope zone with 100-200  $\Omega$ .m of ER. In the downslope zone, a small localized resistive  
9    structure appeared at a distance of 1-2 m from the hedgerow. In the upslope zone a resistive  
10    layer was formed by the unsaturated well-drained organo-mineral A horizons (Fig. 4). Below  
11    this resistive layer, a conductive one was observed with 20-60  $\Omega$  m of ER. The thickness of  
12    this conductive structure decreased and reached the ground surface 4-12 m downslope from  
13    the hedgerow and had a vertical conductive structure below the hedgerow. A third layer with  
14    resistivity ranging from 60 to  $>200$   $\Omega$  m was observed deeply ( $<-2$  m) in the upslope zone and  
15    was shallow downslope from the hedgerow and slightly variable along the slope (Fig. 4).  
16    Over the studied period, a discontinuity in this layer between upslope and downslope zones  
17    appeared vertically below the hedgerow where the lowest resistivity ( $< 20$   $\Omega$  m) was observed  
18    (Fig. 4). Local resistive structures ( $>150$   $\Omega$  m) were observed at cross-section boundaries,  
19    below the ditch and at DW12. These local anomalies were probably due to inversion -method  
20    artefacts.

### 21    **3.2    Time-frame ERT and matric potential profiles**

22    The map of percentage change in electrical resistivity highlights temporal changes in ER  
23    between wet (T06) and dry (T10) states (Fig. 5). This map was compared to matric potential  
24    profiles measured for each location at T06 and T10 (Fig. 5). The map of Fig. 5 and point  
25    measurements highlight two main areas with large differences in ER. From 16 m upslope to 7  
26    m downslope along the toposequence, an increase in ER by 20-100% in the topsoil (0-0.9 m  
27    deep) (Fig. 5). In contrast, ER of the subsoil ( $>1$ m) increased by approximately 20%, with  
28    multiple localized structures in which ER decreased by 20-80%. Below the hedgerow, ER  
29    increased in a three-pronged pattern, with the upslope branch turning down toward the ditch  
30    at  $45^\circ$ , a vertical branch extending beneath the tree, and the downslope branch following the  
31    soil surface. Changes in ER were negative from 7-13 m downslope, but the highest decrease

1 in ER (-80%) was observed 1-4 m upslope below a depth of 2 m. Changes in soil matric  
2 potential corresponded to changes in ER (Fig. 5). According to matric potential data, the  
3 topsoil layer was drier (at depths of 0.25 and 0.5 m) than the subsoil (at depths of 1, 1.5 and 2  
4 m). Soil matric potential decreased upslope at a depth of 0.5 m: from -20 to -152 hPa at 16 m,  
5 -127 to -615 hPa at 8 m and -75 to -425 hPa at 4 m. Under the ditch 1 m upslope and 2 m  
6 downslope, the change in soil matric potential confirmed soil drying down to 1 m and 0.5 m,  
7 respectively. The soil was unsaturated to a depth of 0.40 m at 6 m downslope. Moreover, even  
8 though the soil was saturated by groundwater, electrical resistivity of several localized  
9 structures increased by 5-80% (Fig. 5). These structures were located mainly from 9-11 m and  
10 1-3 m upslope and 1.5-4 m and 11-13 m downslope.

11 Pdfs of ER (Fig. 6a) highlight the shift in mean ER between the entire domain and the topsoil  
12 layer, as do mean values of matric potential Pdf (Fig. 6b). For the topsoil layer, mean ER was  
13 highest when mean matric potential was lowest, corresponding to the driest soil, for both the  
14 wet and dry states. The difference in ER between the entire domain and the topsoil layer was  
15 about 26  $\Omega$  m for T06 (wet state) and reached 110  $\Omega$  m for T10 (Fig. 6a). For matric potential,  
16 the difference between the entire domain and the topsoil layer was about -73 hPa for T06 and  
17 -200 hPa for T10 (Fig. 6b). The greatest changes in both ER and matric potential were located  
18 in the topsoil. In the topsoil layer, change in mean ER and matric potential between the wet  
19 and the dry state was about 120.5  $\Omega$  m and -277 hPa (Fig. 6 a and b), respectively. Pdfs of ER  
20 and Pdfs of matric potential show the same shape between the wet (T06) and dry (T10) state,  
21 with an increase in data dispersion due to the highest amplitude during the dry state (Fig. 6).

### 22 **3.3 Comparison of point measurements: matric potential versus ER**

23 In the unsaturated topsoil, point measurements of matric potential were consistent with ER  
24 extracted from each grid (Fig. 7). Two behaviors were observed for the locations inside and  
25 outside the root zone (Fig. 7). According to the root system pattern (Fig. S2e and S2f, in the  
26 Supplement), we assumed that UP16, UP8 and DW12 were not influenced by the root system  
27 and were thus outside the root zone. The locations assumed to be inside the root zone were  
28 UP4, UP1, DW2 and DW6. For the locations inside and outside (Fig. 7) the root zone, two  
29 different patterns in the relationship between ER and matric potential were observed. Outside  
30 the root zone, a linear relationship was observed ( $R^2=0.8$ ), whereas a dispersion in this  
31 relationship appears for the measurements inside the root zone ( $R^2=0.3$ ). Also, matric

1 potential range measured outside the root zone remained in the same order of magnitude for  
2 both wet and dry states. The wet (T01 to T06 in Fig. 7) and dry (T07 to T10 in Fig. 7) states  
3 were analyzed separately.

4 Upslope, the location situated 4 m from the hedgerow (UP4) showed a pattern similar to those  
5 outside the root zone during the wet state (Fig. 7). UP4 switched to the pattern of the locations  
6 inside the root zone during the dry state (Fig. 7).

### 7 **3.4 VWC estimation**

8 Figure 8 shows relationship between ER and VWC obtained from the WS model with a  
9 standard deviation corresponding to the set of WS parameters. The range of variation in VWC  
10 prediction from the WS model was highest for small ER values ( $<75 \Omega \text{ m}$ ). Outside the root  
11 zone (Fig. 8), VWC values predicted from the retention curve were consistent with VWC  
12 from the WS model both for wet (Fig. 8a) and dry states (Fig. 8b). Inside the root zone (Fig.  
13 8), VWC values predicted from the retention curve were smaller than VWC from the WS  
14 model except for UP4 during the wet state (Fig. 8a). At UP4, VWC predicted from the  
15 retention curve was slightly smaller than that predicted by the WS model during the dry state  
16 (Fig. 8b).

17 Figure 9 shows the relationship between VWC estimated from the retention curve and VWC  
18 predicted by the WS model. Red and gray circles show locations outside and inside the root  
19 zone, respectively. The wet (T01 to T06 in Fig. 9) and dry (T07 to T10 in Fig. 9) states were  
20 analyzed separately. For the both wet and dry states, the relationship between the two  
21 predictions had a strong correlation ( $r=0.9$ ) for locations outside the root zone. Predictions for  
22 UP4 were quite good, especially for the wet state (Fig. 9). During the dry state, the  
23 relationship between the two predictions remained acceptable, with a smaller VWC from the  
24 retention curve (Fig. 9). A shift between the locations inside and outside the root zone  
25 indicates two different patterns. VWC values predicted from the WS model show highest soil  
26 moisture for locations inside the root zone (Fig. 9).

## 27 **4 DISCUSSION**

28 Predicting VWC from ERT has become a classical approach widely used by geophysicists.  
29 The method developed has several steps summarized on (Fig. 10), from data acquisition to  
30 processing. ERT, matric potential, and groundwater level measurements were performed over  
31 the studied period. PSD, bulk and root density were also characterized along the

1 toposéquence. Changes in ER over time were predicted without removing the effect of soil  
2 temperature variations over the study period, since these data were missing. Pdfs of ER and  
3 matric potential were helpful for analyzing the statistical range of data and selecting the  
4 relevant monitoring time. The most contrasting times, corresponding to the wettest (T06) and  
5 driest (T10) states, were analyzed. ER and matric potential data from the unsaturated zone  
6 were extracted to analyze the relationship between ER and matric potential (Fig. 10). ER  
7 measurements were also converted to VWC by a simplified petro-physical model of Waxman  
8 and Smits. VWC was also predicted using retention curves (Fig. 10). Outside the root zone,  
9 the same relationships between ER and respectively VWC, and matric potential were  
10 observed for the wet and dry periods. Inside the root zone, a non-stationarity on those  
11 relationships was observed (Fig. 10).

#### 12 **4.1 Soil properties and horizons organization**

13 Vertically, ER maps revealed three main structures along the toposéquence: (i) a resistive  
14 topsoil layer (Figs. 4 and S5) underlying the well-drained organo-mineral A horizon in the  
15 upslope zone, (ii) stagnic (A) and endostagnic (E, B) horizons that are more conductive (Figs.  
16 4 and S5), (iii) deep C mineral horizon with intermediate ER (Figs. 4 and S5) and  
17 irregular structures that were probably related to the degree of weathering of the Brioverian  
18 schist.

19 The three main structures are intersected by a vertical conductive structure below the  
20 hedgerow (Figs. 4 and S5). We hypothesized that this structure may result from a higher  
21 degree of bedrock weathering caused by the main taproot (Baffet, 1984). The increase with  
22 clay content due to bedrock weathering caused ER to decrease in the vertical conductive  
23 structure. Near the taproot, preferential water flow also contributes to bedrock weathering.

24 As expected, our results show that lateral and vertical changes in ER are consistent with clay  
25 content measurements at multiple depths (Ward, 1990). In the downslope zone, clay content is  
26 4-6% higher than upslope zone (Ghazavi et al., 2008). In addition, clay content increased and  
27 ER decreased with depth for all upslope locations (UP16, UP8, and UP4). ER also decreased  
28 when soil bulk density increased from the topsoil to the depth of the unsaturated zone (Figs.  
29 S2a and S2b). Besson et al. (2004) obtained similar results, indicating that soil ER was  
30 sensitive to bulk density. An increase in bulk density from 1.39 to 1.59 in a loamy soil  
31 corresponded to an 11  $\Omega$  m decrease in ER (Besson et al., 2004).

## 1 **4.2 Spatial distribution of hedgerow roots in the unsaturated zone**

2 Most roots were located in the upslope zone from 0.1-1.0 m deep (61% from 0.1-0.5 m deep  
3 and 36% from 0.5-1.0 m deep) and extended up to 6 m upslope from the hedgerow (Figs. S2e  
4 and S2f). Downslope, 92% of roots were located from 0.1-0.5 m deep and only 8% were  
5 located from 0.5-1.0 m deep (Figs. S2e and S2f). In addition, oak roots did not extend further  
6 than 9 m downslope. The temporal change in ER was largest in the topsoil layer and inside  
7 the root zone (Fig. 5a). Also, matric potential gradients between 2 depths, were highest near  
8 the hedgerow (Fig. 5b). They were induced by root water uptake and agree with the literature  
9 on the spatial distribution of oak root systems (Drénou, 2006; Lucot, 1994). In our study, the  
10 spatial distribution of the root system was influenced by soil characteristics and anthropogenic  
11 features such as the ditch and the embankment on which the hedgerow was planted.  
12 Investigation of root depth along the toposequence was limited by a compact soil layer with a  
13 high bulk density of 1.6 (Fig. S2 a and b, in the Supplement) starting at a depth of 0.6 m.  
14 In agreement with previous observations (Amato et al., 2008; Al Hagrey, 2007; Rossi et al.,  
15 2011), our results show several highly resistive areas close to the tree trunk (Figs. 4 and  
16 S5). Increases in ER between the wet and dry states (Fig. 5) likely identify the spatial limits of  
17 the hedgerow root system highlighting a three-pronged pattern inside the root zone. Rossi et  
18 al. (2011) demonstrated that ER variability in an orchard was related only to root biomass  
19 density. In our experiment, quantitative analysis of the relationship between ER and root  
20 density was not relevant, since their locations in the toposequence were not exactly the same.

## 21 **4.3 Consistency between ER and matric potential**

22 Changes in ER are related to parameters such as volumetric water content, solute  
23 concentration and temperature (Ward, 1990). According to our experimental design, changes  
24 in ER were compared to those in soil matric potential, which were converted into volumetric  
25 water content by using measured retention curve (section 4.4).

26 Two different behaviors in the relationship between ER and matric potential were observed  
27 between locations outside the root zone (UP16, UP8, and DW12) and those inside the root  
28 zone (UP4, UP1, DW2 and DW6), with  $R^2$  values of 0.8 and 0.3, respectively (Fig. 7).  
29 However, for UP4, this relationship adequately fit the curve obtained outside the root zone  
30 during the wet state (T01-T06). Despite high root density, UP4 showed the same behavior as  
31 the locations outside the root zone. The wet and leafless period, which occurred from autumn  
32 to the beginning of spring, without transpiration (Thomas et al., 2012), was characterized by



1 no influence from the root system. The ER-matric potential relationship of UP4 followed the  
2 locations outside the root zone during the wet state. For the dry state, ER values doesn't  
3 change despite of a change in matric potential. For this location, decrease in matric potential  
4 was related to a small change in ER values. Inside the root zone, the relationship between  
5 matric potential and ER had high variability from wet to dry states, probably caused by soil  
6 heterogeneity (Fig. 7). A decrease in matric potential (from -100 to -650 hPa) inside the root  
7 zone was related to a small change in ER. At our study site, the hedgerow with a bank and a  
8 ditch increased soil variability (Fig. 1). Moreover, as described by Hesse (1990), variation in  
9 topography modifies bulk ER measurements for a given electrode array. For a homogenous  
10 soil system, bulk ER decreases over a bank and increases over a ditch (Hesse, 1990).  
11 Topographical singularities create anomalies in ER values.  
12 The ability of ER to predict soil matric potential was quite good along the toposequence  
13 outside the root zone (Fig. 7). We hypothesized that the many singularities around the  
14 hedgerow, combined with the high root density, increased the signal-to-noise ratio.  
15 Considering the shift in mean ER (Pdf in Fig. 6a) between the wettest (T06) and driest (T10)  
16 states, the decrease in matric potential did not change the shape of ER distributions but only  
17 their mean values, which was highest when the soil was drier. Matric potential profiles (Fig.  
18 5b) showed a drier zone inside the root zone.

#### 19 **4.4 VWC prediction using ER inside and outside the root zone**

20 By analyzing 27 simulations from the WS model, our results highlight the sensitivity of VWC  
21 prediction to WS parameters (standard deviation = 0.030- 0.014%). Outside the root zone,  
22 VWC values predicted by the WS model were consistent with those from the retention curve  
23 (Fig. 8), suggesting the ability of ER to predict soil moisture in a homogenous soil system.  
24 Differences in VWC prediction inside the root zone were observed for both wet and dry states  
25 (Fig. 8). Moreover, ER values were smaller than 50  $\Omega$  m, indicating limitations of the WS  
26 model. As suggested by (Laloy et al., 2011), among five petro-physical models tested on a  
27 loamy soil to predict VWC and soil bulk density, the Waxman and Smits model appeared  
28 more consistent for electrical resistivity values  $> 100\Omega$ m which are often observed in dry  
29 soils. For lower ER values ( $<100\Omega$ m), the volume-averaging method (Pride, 1994; Linde et  
30 al., 2006) outperformed other tested models. In our study, the bad results obtained from WS  
31 model are probably related to the inconsistency in parameters as soil water electrical  
32 conductivity changes with soil moisture inside the root zone. Outside the root zone, a good

1 agreement between WS and retention curve predictions during the wet state highlights the  
2 ability of ER to predict soil moisture (Fig. 9). A linear relationship was observed between  
3 VWCs predicted by the WS model and the retention curve. Inside the root zone, VWC  
4 predicted with the WS model overestimated soil moisture for both wet and dry states.  
5 Overestimation of soil moisture inside the root zone was probably related to soil  
6 heterogeneity. Also, shallow groundwater up to 2 m deep maintained a relatively wet soil  
7 along the toposéquence. No change in water content occurred, since the all pores of the  
8 saturated zone were occupied by water. We conclude that changes in ER were probably  
9 related to changes in electrical conductivity of soil water. We also observed a high chloride  
10 concentration below the hedgerow in the same toposequence (Grimaldi et al., 2009). It is well  
11 known that ER decreases when ionic concentration increases (Ward, 1990). Since chloride is  
12 a conservative solute, its concentration increased with water and nutrient uptake. At this  
13 location, the highly conductive structures (Figs. 4 and S5) were observed below the  
14 hedgerow, in agreement with observations of chloride concentration (Grimaldi et al., 2009).  
15 These structures, probably due to a high chloride concentration, moved little over time on the  
16 ER maps (T01 to T10, Fig. S5). The conductive structure observed at UP1 from T01 to T04  
17 disappeared at T05 due to high rainfall (Figs. 2a and S5). Rainfall events observed between  
18 T04 and T05 should have diluted solutes. Another conductive structure below the hedgerow  
19 appeared at T07 and at T09, when root water uptake was highest. Change in conductive zones  
20 and their small degree of movement was probably related to water fluxes and chloride  
21 concentration.

22 To analyze the relationship between soil ER and individual parameters, further studies are  
23 needed. High-resolution analysis should be performed by monitoring chloride concentration,  
24 ER, and soil matric potential at the same spatial (grid size) and temporal resolutions. In this  
25 way, the perspective of using ER maps as a proxy for chloride accumulation in the vadose  
26 zone could be addressed.

27 The originality of our approach consists in analyzing both spatial and temporal effects of soil  
28 moisture. Spatial effects of the root zone induced a non-stationarity of the relationship  
29 between VWC (or  $\psi$ ) and ER (Fig. 10) for dry and wet periods. The temporal effect was  
30 mainly controlled by the seasonality (wet and the dry periods), which is well known as a first-  
31 order forcing.

32

## 1 **5 CONCLUSION**

2 ERT monitoring offers a non-invasive tool with a high resolution, providing information  
3 about soil horizon geometry as well as physical and chemical properties. The geophysical  
4 signal reveals combined contributions from the main parameters (i.e. structure, water content,  
5 fluid composition), but their individual effects are more difficult to assess.

6 The hydrological year studied was particularly wet. The Pdfs of ER and matric potential  
7 measurements for wettest and driest states show the largest difference in mean values in the  
8 topsoil layer. The relationship between ER and matric potential highlights different trends  
9 inside and outside the root zones. Also, the heterogeneous zone, below the hedgerow,  
10 identified using ER changes and matric potential profiles, were consistent with vertical and  
11 horizontal root density. Two different behaviors for locations inside and outside the root zone  
12 were identified. A strong correlation between VWC values predicted by the Waxman and  
13 Smits model and those obtained by the retention curve was observed outside the root zone  
14 ( $r=0.9$ ). In contrast, ER and soil moisture have a weak correlation at the hedgerow proximity.  
15 A shift in the VWC from Waxman and Smith and retention curve was observed inside the  
16 root zone revealing the non-stationarity in this relationship between wet and dry periods. The  
17 non-unequivocal of this relationship show the limitation of using ER to predict soil moisture  
18 in heterogeneous soil system. Similar monitoring with ERT should be extended to a variety of  
19 toposequences with contrasting interaction between topography and soil structures on the  
20 rhizosphere. More investigations of heterogeneous soil systems would help to determine if  
21 ERT measurements are appropriated to predict soil moisture of heterogeneous soil systems. In  
22 many hedgerow landscapes where the density of linear vegetation structure is high,  
23 heterogeneities on the rhizosphere are mainly due to human activities which modify  
24 landscapes by creating topographical singularities such as ditches and banks. In the particular  
25 topographical context of our case study, soil heterogeneities inside the root zone are mainly  
26 related to the high root density below the ditch-bank-hedgerow system. Such systems are  
27 commonly encountered in Brittany and throughout northwestern Europe.

28

## 29 **Acknowledgements**

30 Part of this work was supported by the ECOGER project ACI Ecco. The authors thank INRA  
31 and AGROCAMPUS OUEST for supporting this research. The Mogis and Courtillon families  
32 kindly accepted the installation of experimental equipment on their fields.

1  
2  
3  
4  
5  
6  
7  
8  
9  
10  
11  
12  
13  
14  
15  
16  
17  
18  
19  
20  
21  
22  
23  
24  
25  
26  
27  
28

**References**

Adam, I., Michot, D., Guero, Y., Soubega, B., Moussa, I., Dutin, G., and Walter, C.:  
Detecting soil salinity changes in irrigated Vertisols by electrical resistivity prospection  
during a desalinisation experiment, *Agricultural and Water Management.*, 109, 1-10,  
doi:10.1016/j.agwat.2012.01.017, 2012.

Al Hagrey, S.A.: Geophysical imaging of root-zone, trunk, and moisture heterogeneity, *J.  
Exp. Bot.*, 58, 839-54, doi:10.1093/jxb/erl237, 2007.

Al Hagrey, S.A. and Michaelson, J.: Resistivity and percolation study of preferential flow in  
vadose zone at Bokhost, Germany, *Geophysics*, 64, 746-753, 1999.

Al Hagrey, S.A. and Petersen, T.: Numerical and experimental mapping of small root zones  
using optimized surface and borehole resistivity tomography, *Geophysics*. 76, 25-35,  
2011.

Amato, M., Basso, B., Celano, G., Bitella, G., Morelli, G., and Rossi, R.: In situ detection of  
tree root distribution and biomass by multi-electrode resistivity imaging, *Tree Physiol*,  
28, 1441-1448, 2008.

Amato, M., Bitella, G., Rossi, R., Gómez, J.A., Lovelli, S., and Gomes, J.J.F.: Multi -  
electrode 3D resistivity imaging of alfalfa root zone, *Eur. J. Agron*, 31, 213–222,  
doi:10.1016/j.eja.2009.08.005, 2009.

Archie, G. E.: The electrical resistivity log as an aid in reservoir characteristics, *Transactions  
of the AIME*, 146, 54–62, 1942.

Baffet, M. : Influence de la haie sur l'évolution des caractères physico-chimiques et  
hydrodynamiques des sols, Thèse de doctorat de l'Université de Limoges, 1984.

Beff, L., Günther, T., Vandoorne, B., Couvreur, V., and Javaux, M.: Three-dimensional  
monitoring of soil water content in a maize field using Electrical Resistivity  
Tomography, *Hydrol. Earth Syst. Sci.*, 17, 595–609, doi:10.5194/hess-17-595-2013,  
2013.

- 1 Besson, A., Cousin, I., Samouëlian, A., Boizard, H., and Richard, G.: Structural heterogeneity  
2 of the soil tilled layer as characterized by 2D electrical resistivity surveying, *Soil and*  
3 *Tillage Research*, 79, 239-249, 2004.
- 4 Bréda, N., Granier, A., Barataud, F., and Moyne, C.: Soil-water dynamic in an oak stand. I.  
5 Soil moisture, water potentials, and water uptake by roots, *Plant and Soil*, 172, 17-27,  
6 1995.
- 7 Brillante, L., Bois, B., Mathieu, O., Bichet, V., Michot, D., and Lévêque, J.: Monitoring soil  
8 volume wetness in heterogeneous soils by electrical resistivity. A field-based  
9 pedotransfer function, *J. Hydrol.*, 516, 55–66, doi:10.1016/j.jhydrol.2014.01.052, 2014.
- 10 Brillante, L., Mathieu, O., Bois, B., Van Leeuwen, C., and Lévêque, J.: The use of soil  
11 electrical resistivity to monitor plant and soil water relationships in vineyards, *SOIL*, 1,  
12 273-286, 2015.
- 13 Caubel, V.: Influence de la haie de ceinture de fond de vallée sur les transferts d'eau et de  
14 nitrate. Thèse de Doctorat de l'Ecole Nationale des Sciences Agronomiques de Rennes,  
15 2001.
- 16 Decagon Devices.: Mini disk infiltrometer, Model S, user's manual version3, Decagon  
17 devices, Pullman, WA, 2006.
- 18 Descloitres, M., Ribolzi, O., Le Troquer, Y., and Thiébaux., J. P.: Study of water tension  
19 differences in heterogeneous sandy soils using surface ERT, *Journal of Applied*  
20 *Geophysics*, 64, 83–98, 2008.
- 21 Drénou, C.: Les racines, face cachée des arbres., Institut pour le développement forestier,  
22 Paris, 2006.
- 23 FAO: World Reference Base for Soil Resources, IUSS Working Group, 2nd edition FAO,  
24 World Soil Resources Report No. 103, FAO, Rome, 2006.
- 25 Ferren, J.C. : Monographie du climat, Station de Rennes-Le Rheu, Analyse sur 30 années des  
26 moyennes mensuelles 1971-2000, INRA, Rennes, 2004.
- 27 Follain, S., Walter, C., Bonté, P., Marguerie, D., and Lefevre, I.: A-horizon dynamics in a  
28 historical hedged landscape, *Geoderma.*, 150, 334-343, 2009.
- 29 Garré, S., Javaux, M., Vanderborght, J., Pagès, L., and Vereecken, H.: Three-dimensional

- 1 electrical resistivity tomography to monitor root zone water dynamics, *Vadose Zone J.*, 10,  
2 412-424, 2011.
- 3 Garré, S., Günther, T., Diels, J., and Vanderborght, J.: Evaluating experimental design of ERT  
4 for soil moisture monitoring in contour hedgerow inter-cropping systems, *Vadose Zone*  
5 *J.*, 11 (4), 2012.
- 6 Garré, S., Coteur, I., Wongleecharoen, C., Kongkaew, T., Diels, J., and Vanderborght, J.:  
7 Noninvasive monitoring of soil water dynamics in mixed cropping systems. A case study  
8 in Ratchaburi Province, Thailand, *Vadose Zone J.*, 12 (2), 2013.
- 9 Ghazavi, G., Thomas, Z., Hamon, Y., Marie, J.C., Corson, M., and Merot, P.: Hedgerow  
10 impacts on soil-water transfert due to rainfall interception and root-water uptake.  
11 *Hydrological Processes*, 22, 4723-4735, 2008.
- 12 Grimaldi, C., Thomas, Z., Fossey, M., Fauvel, Y., and Merot, P.: High chloride  
13 concentrations in the soil and groundwater under an oak hedge: an indicator of  
14 evapotranspiration and water movement, *Hydrological processes*, 23, 1865-1873, 2009.
- 15 Ghazavi, G., Thomas, Z., Hamon, Y., and Merot, P.: Spatial and temporal variation of soil-  
16 water movement under a hillslope hedgerow during contrasting meteorological  
17 conditions, *Hydrological Processes*, 25, 1431-1442, 2011.
- 18 Hadzick, Z. Z., Guber, A. K., Pachepsky, Y. A., and Hill, R. L.: Pedotransfer functions in soil  
19 electrical resistivity estimation, *Geoderma*, 164, 195–202, doi:10.1016/  
20 j.geoderma.2011.06.004, 2011.
- 21 Hesse, A.: Resistivity prospecting, in: Scollar, I., Tabbagh, A., Hesse, A., and Herzog, I.,  
22 (Eds.), *Archaeological prospecting and remote sensing*, Cambridge University Press,  
23 Cambridge, 307-374, 1990.
- 24 Laloy, E., Javaux, M., Vanclooster, M., Roisin, C., and Bielders, C. L.: Electrical resistivity in  
25 a loamy soil: identification of the appropriate pedo-electrical model, *Vadose Zone J.*, 10,  
26 1023–1033, doi:10.2136/vzj2010.0095, 2011.
- 27 Linde, N., Binley, A., Tryggvason, A., Pedersen, L.B., and Revil, A.: Improved  
28 hydrogeophysical characterization using joint inversion of crosshole electrical resistance  
29 and ground-penetrating radar travelttime data, *Water Resour. Res.*, 42, W12404.  
30 doi:10.1029/2006WR005131, 2006.

- 1 Loke, M.H. and Barker, R.D.: Rapid least-squares inversion of apparent resistivity  
2 pseudo-sections by a quasi-Newton method, *Geophysical Prospecting*, 44,131-152.  
3 1996.
- 4 Lucot, E. : Influence des caractéristiques de la piérorosité des sols sur la prospection racinaire  
5 et l'alimentation hydrique des arbres. Application à l'estimation de la valeur des sols  
6 forestiers, Thèse de doctorat de l'Université de Franche-Comté, 1994.
- 7 Michot, D.: Intérêt de la géophysique de subsurface et de la télédétection multispectrale pour  
8 la cartographie des sols et le suivi de leur fonctionnement hydrique à l'échelle  
9 intraparcellaire, Thèse de l'Université Paris VI, 2003.
- 10 Michot, D., Dorigny, A., and Benderitter. Y.: Determination of water flow direction and corn  
11 roots-induced drying in an irrigated Beauce CALCISOL, using electrical resistivity  
12 measurements, *Comptes Rendus De L'Academie Des Sciences Serie II Fascicule a-*  
13 *Sciences De La Terre Et Des Planetes*, 332, 29–36, 2001.
- 14 Michot, D., Benderitter, Y., Dorigny, A., Nicoullaud, B., King, D., and Tabbagh. A.: Spatial  
15 and temporal monitoring of soil water content with an irrigated corn crop cover using  
16 surface electrical resistivity tomography, *Water Resour. Res*, 39, 1138–1158, 2003.
- 17 Müller, K., Vanderborght, J., Englert A., Kemna, A., Huisman, J.A., Rings, J., and  
18 Vereecken, H.: Imaging and characterization of solute transport during two tracer tests in  
19 a shallow aquifer using electrical resistivity tomography and multilevel groundwater  
20 samplers, *Water Resour. Res*, 46(3), 1-23, W03502. doi:10.1029/2008WR007595, 2010.
- 21 Nijland, W., van der Meijde, M., Addink, E.A., and de Jong, S.M.: Detection of soil moisture  
22 and vegetation water abstraction in a Mediterranean natural area using electrical  
23 resistivity tomography, *Catena*, 81, 209–216, 2010.
- 24 Pride, S.: Governing equations for the coupled electromagnetics and acoustics of porous  
25 media, *Phys. Rev.*, B 50,15678–15696, doi:10.1103/PhysRevB.50.15678, 1994.
- 26 Rossi, R., Amato, M., Bitella, G., Bochicchio R., Ferreira Gomes, J.J., Lovelli, S., Martorella,  
27 E., and Favale, P.: Electrical resistivity tomography as a nondestructive method for  
28 mapping root biomass in an orchard, *Eur. J. Soil Sci*, 62, 206–215, doi:10.1111/j.1365-  
29 2389.2010.01329.x, 2011.
- 30 Samouëlian A., Cousin, I., Tabbagh A., Bruand, A., and Richard, G.: Electrical resistivity  
31 survey in soil science: a review, *Soil and Tillage Research*, 83, 173-193, 2005.

- 1 Srayeddin, I. and Doussan, C.: Estimation of the spatial variability of root water uptake of  
2 maize and sorghum at the field scale by electrical resistivity tomography, *Plant Soil*, 319,  
3 185–207, 2009.
- 4 Thomas, Z., Molénat, J., Caubel, V., Grimaldi, C., and Mérot P.: Simulating soil-water  
5 movement under a hedgerow surrounding a bottomland reveals the importance of  
6 transpiration in water balance, *Hydrol Process*, 22, 577-585, 2008.
- 7 Thomas, Z., Ghazavi, R., Merot, P., and Granier, A.: Modelling and observation of hedgerow  
8 transpiration effect on water balance components at the hillslope scale in Brittany, *Hydrol*  
9 *Process*, 26, 4001–4014, 2012.
- 10 Van Genuchten, M.T.: A Closed-form equation for predicting the hydraulic conductivity of  
11 unsaturated soils, *Soil Sci. Soc. Am. J.*, 44 (5), 892-898, 1980.
- 12 Walter, C., Mérot, P., Layer, B., and Dutin, G.: The effect of hedgerows on soil organic  
13 carbone storage in hillslopes, *Soil Use and Management*, 19, 201-207, 2003.
- 14 Ward, S.H: Resistivity and induced polarization methods, in: Ward, S.H. (Ed), *Investigations*  
15 *in Geophysics N°5, Geotechnical and Environmental Geophysics*, Society of Exploration  
16 *Geophysicists*, Tulsa, Oklahoma, 1990.
- 17 Waxman, M. H. and Smits, L. J. M.: Electrical conductivities in oil-bearing shaly sands, *Soc.*  
18 *Pet. Eng. J.*, 8, 107–122, doi:10.2118/1863-A, 1968.
- 19 Werban, U., al Hagrey, S.A., and Rabbel,W.: Monitoring of root-zone water content in the  
20 laboratory by 2D geoelectrical tomography, *J. Plant Nutr. Soil Sci*, 171, 927–935, 2008.
- 21 Wooding, R.A.: Steady infiltration from a shallow circular pond, *Water Resour. Res.*, 4,  
22 1259–1273, 1968.
- 23 Yamakawa, Y., Kosugi, K., Katsura, N., Masaoka, N., and Mizuyama, T.: Spatial and  
24 temporal monitoring of water content in weathered granitic bedrock using electrical  
25 resistivity imaging, *Vadose Zone J.*, 11, 2012.
- 26 Zenone, T., Morelli, G., Teobaldelli, M., Fischanger, F., Matteucci, M., Sordini, M., Armani,  
27 A., Ferre, C., Chiti, T., and Seufert. G.: Preliminary use of groundpenetrating radar and  
28 electrical resistivity tomography to study tree roots in pine forests and poplar plantations.  
29 Commonwealth Scientific and Industrial Research Organization, Collingwood, Australia.  
30 2008.



1 Zhou, Q.Y., Shimada, J., and Sato, A.: Three-dimensional spatial and temporal monitoring of  
2 soil water content using electrical resistivity tomography, *Water resources research*, 37,  
3 273-285, 2001.  
4

1 **Tables and Figures**

2 Table 1. Parameters used to predict volumetric water content in the Waxman and Smits  
3 model. Sensitivity analysis of WS using 27 simulations (for N parameters and m values,  
4 simulation number = $N^m$ ).

5

	<b>a (S m<sup>-1</sup>)</b>	<b>b (S m<sup>-1</sup>)</b>	<b>n</b>
Value 1	0.059	1.00E-03	1.0356
Value 2	0.080	1.00E-03	1.1271
Value 3	0.150	1.00E-03	1.3996

6

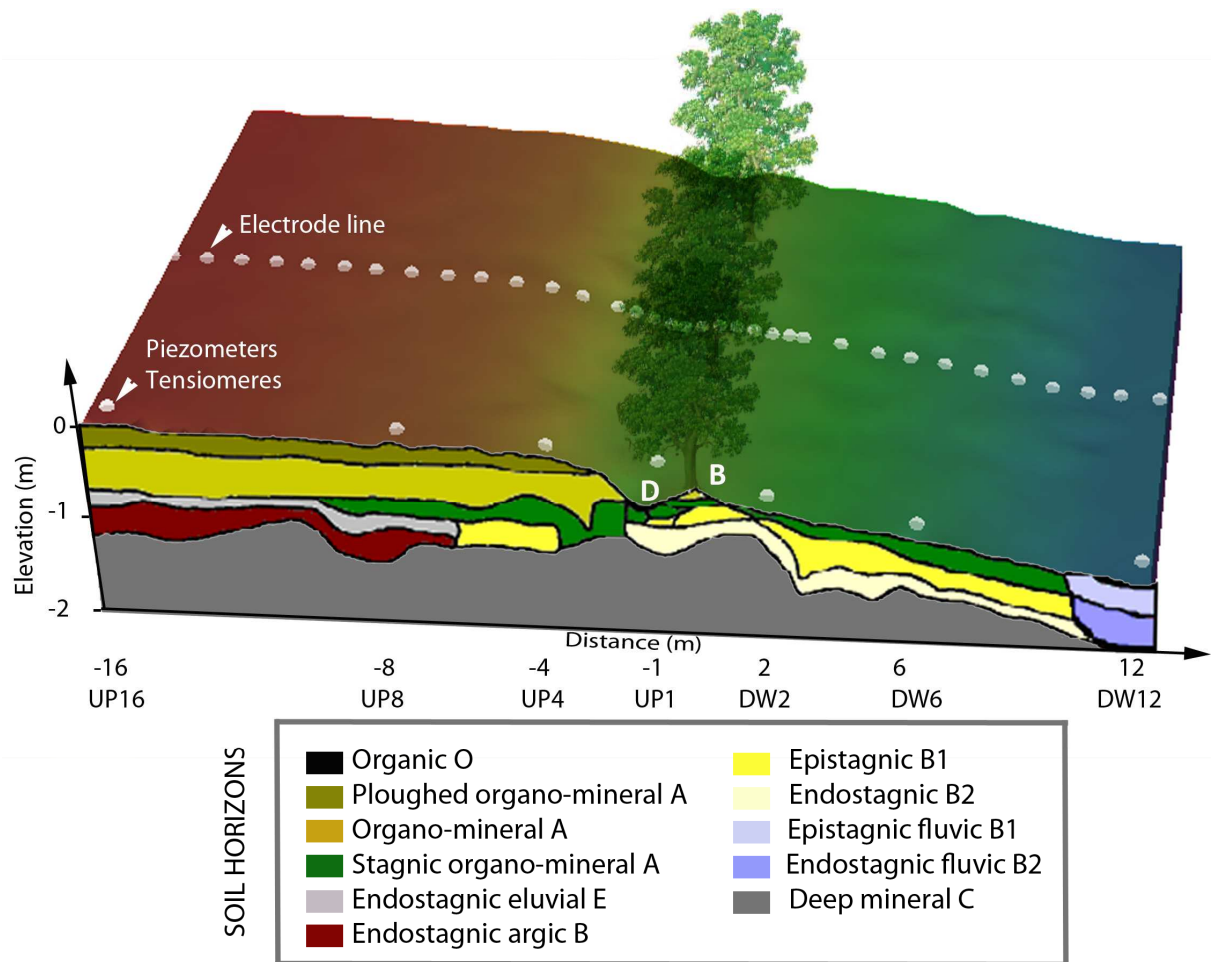
1 Table 2. Statistics of electrical resistivity measurements calculated from the 548 cells of the  
 2 entire 2D section (entire domain) at each monitoring time (T01 to T10) of electrical resistivity  
 3 tomography.

4

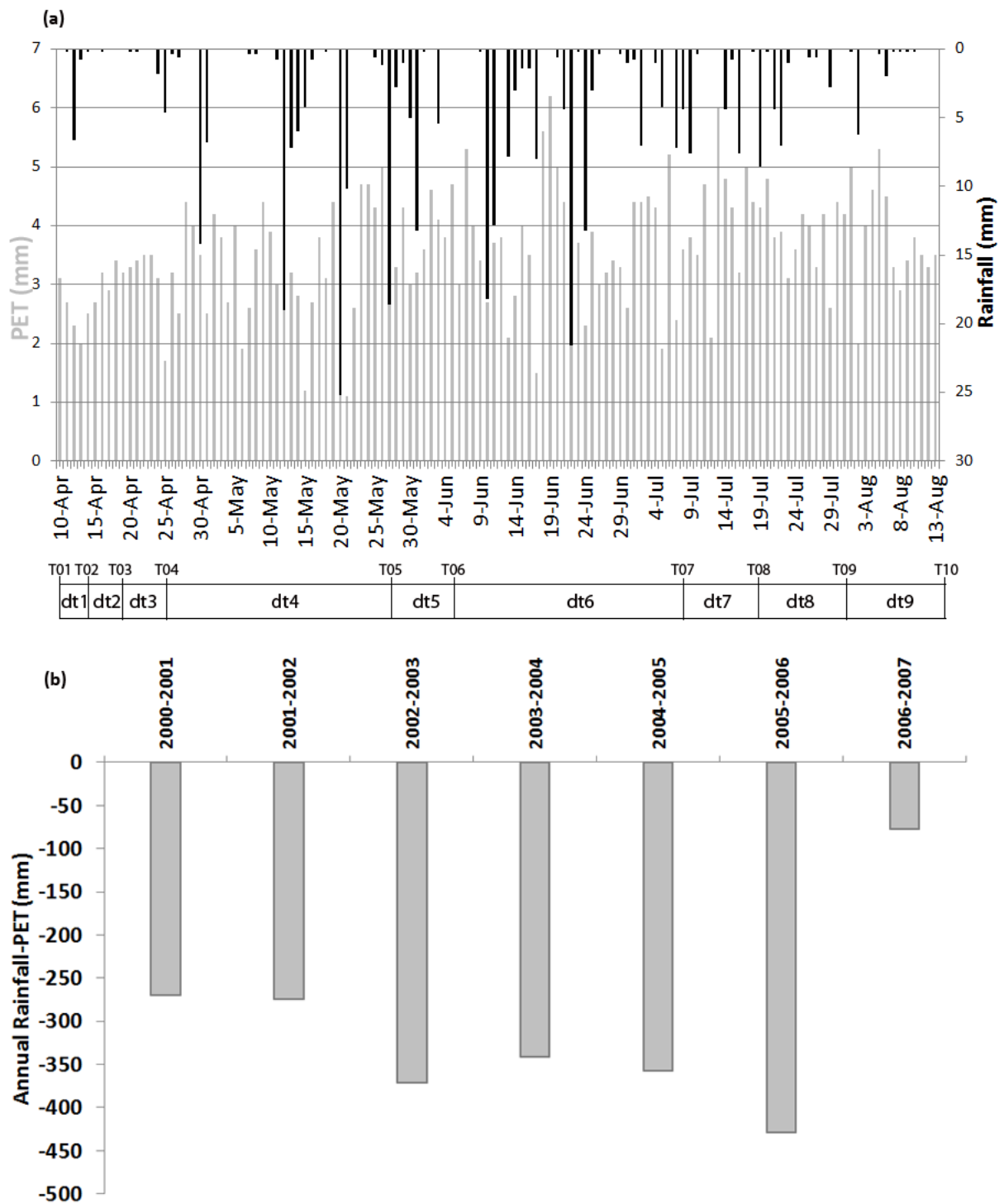
Electrical resistivity ( $\Omega$ m)	<b>T01</b>	<b>T02</b>	<b>T03</b>	<b>T04</b>	<b>T05</b>	<b>T06</b>	<b>T07</b>	<b>T08</b>	<b>T09</b>	<b>T10</b>
Minimum	9.2	10.5	10.9	11.8	10.6	10.7	11.4	11.7	12.1	9.3
Maximum	615.2	436.3	386.8	493.0	413.5	382.9	344	354.8	384.1	722.9
Standard Deviation	63.7	61.6	59.9	63.3	53.0	52.6	57.2	57.0	60.6	99.2
<b>Mean</b>	<b>89.2</b>	<b>88.6</b>	<b>86.7</b>	<b>88</b>	<b>78.5</b>	<b>78</b>	<b>80.8</b>	<b>80</b>	<b>83</b>	<b>104.3</b>
<b>Median</b>	<b>74.4</b>	<b>71.9</b>	<b>68.6</b>	<b>68.8</b>	<b>66.4</b>	<b>65.4</b>	<b>64.4</b>	<b>64.7</b>	<b>66.4</b>	<b>73.5</b>

5

6



1  
 2 Figure 1. Experimental setup and soil horizon organization along the toposequence. Soil was  
 3 excavated up from 16 m upslope (UP16) to 12 m downslope (DW12). Soil horizons are  
 4 named according to the World Reference Base for Soil Resources (FAO, 1998). D and B  
 5 indicate respectively ditch and bank locations. Each monitored location (UP16, UP8, UP4,  
 6 UP1, DW2, DW6 and DW12) was equipped with 5 tensiometers and 1 piezometer.

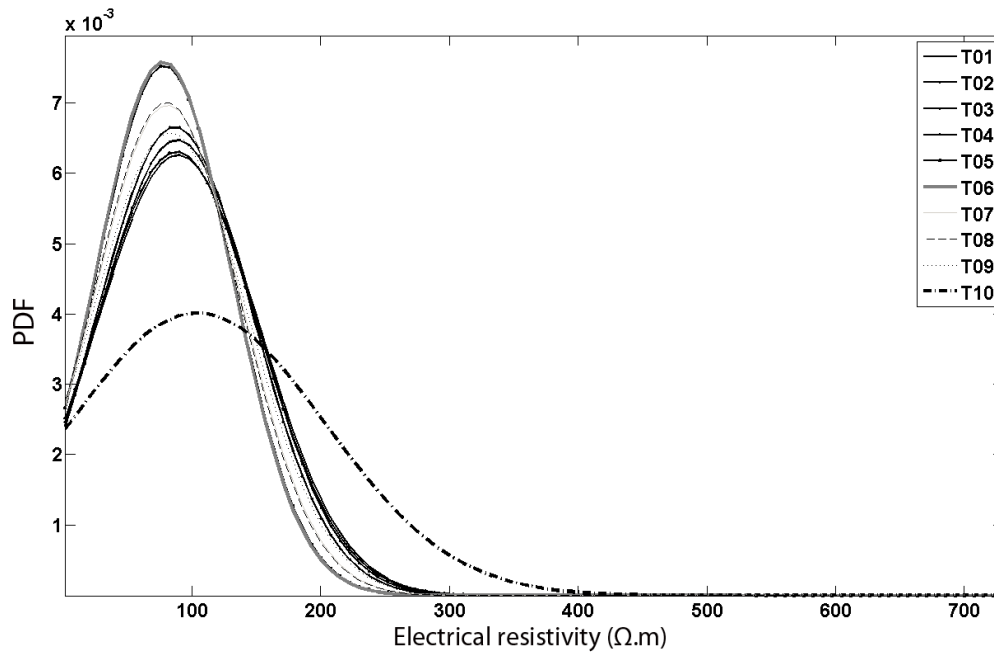


1

2 Figure 2. (a) Daily rainfall and potential evapotranspiration (PET) measured during the  
 3 monitoring period (10 April to 13 August 2007). ERT measurement dates (T01 to T10) and  
 4 intervals between them (dt1 to dt10) are indicated along the x axis. (b) Annual net rainfall  
 5 (rainfall - PET) calculated for the previous 6 years. Annual net rainfall calculated for each  
 6 interval of the monitoring period and compared to those of the previous 6 years is presented in  
 7 the supplements (Fig. S1).

1

2



3

4

5

6 Figure 3. Probability density functions (Pdf) estimated from electrical resistivity  
7 measurements of the entire 2D section at each date of electrical resistivity tomography.  
8 Curves were fitted with a Gaussian model.

9

10

11

12

13

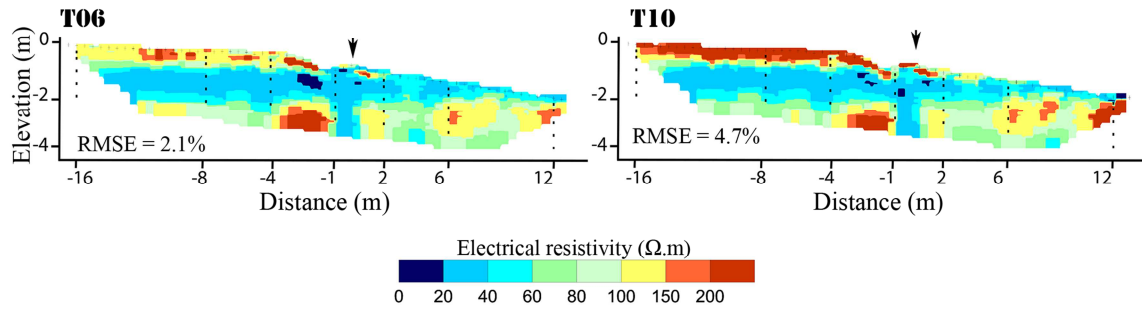
14

15

16

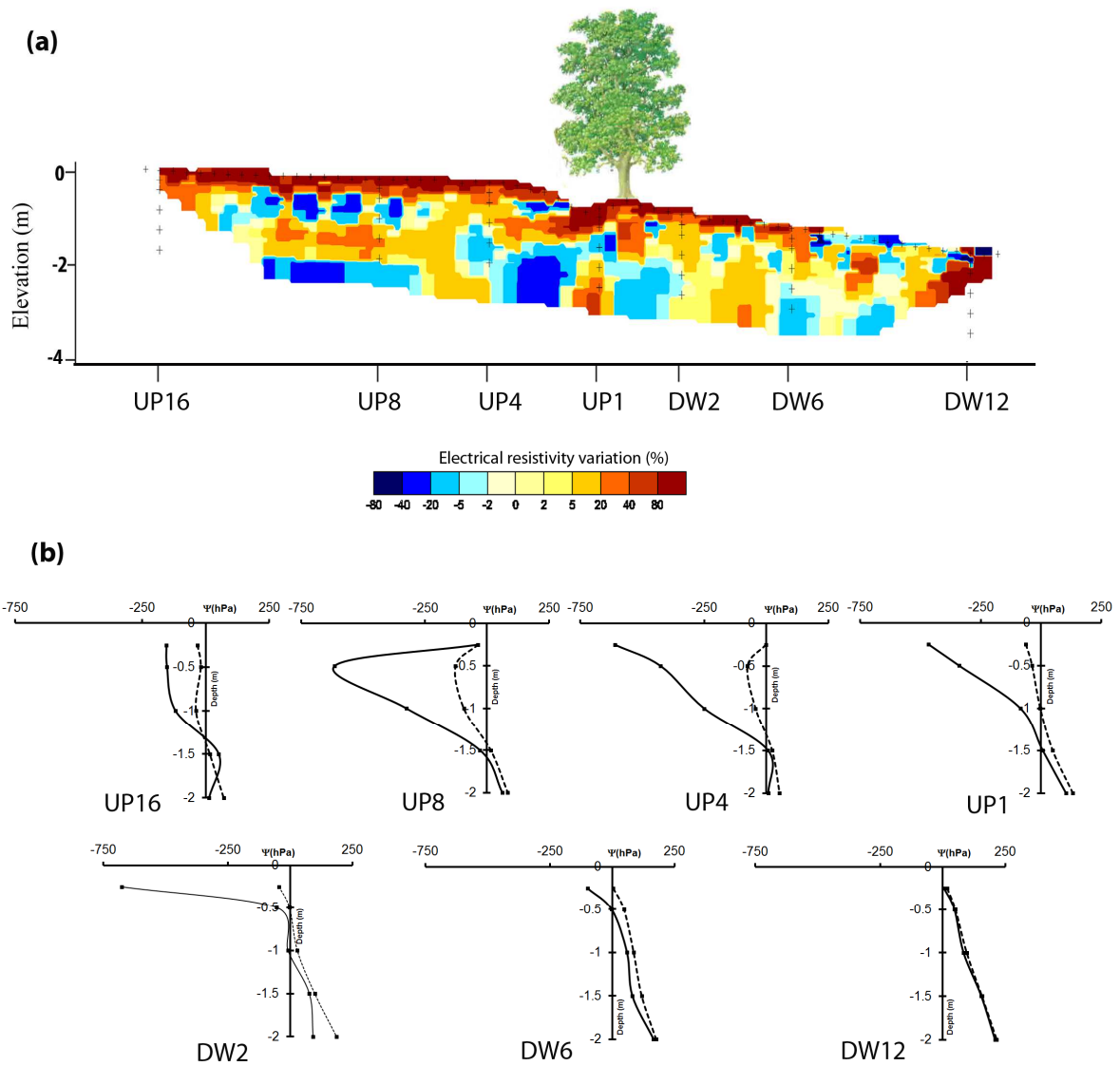
17

1  
2  
3



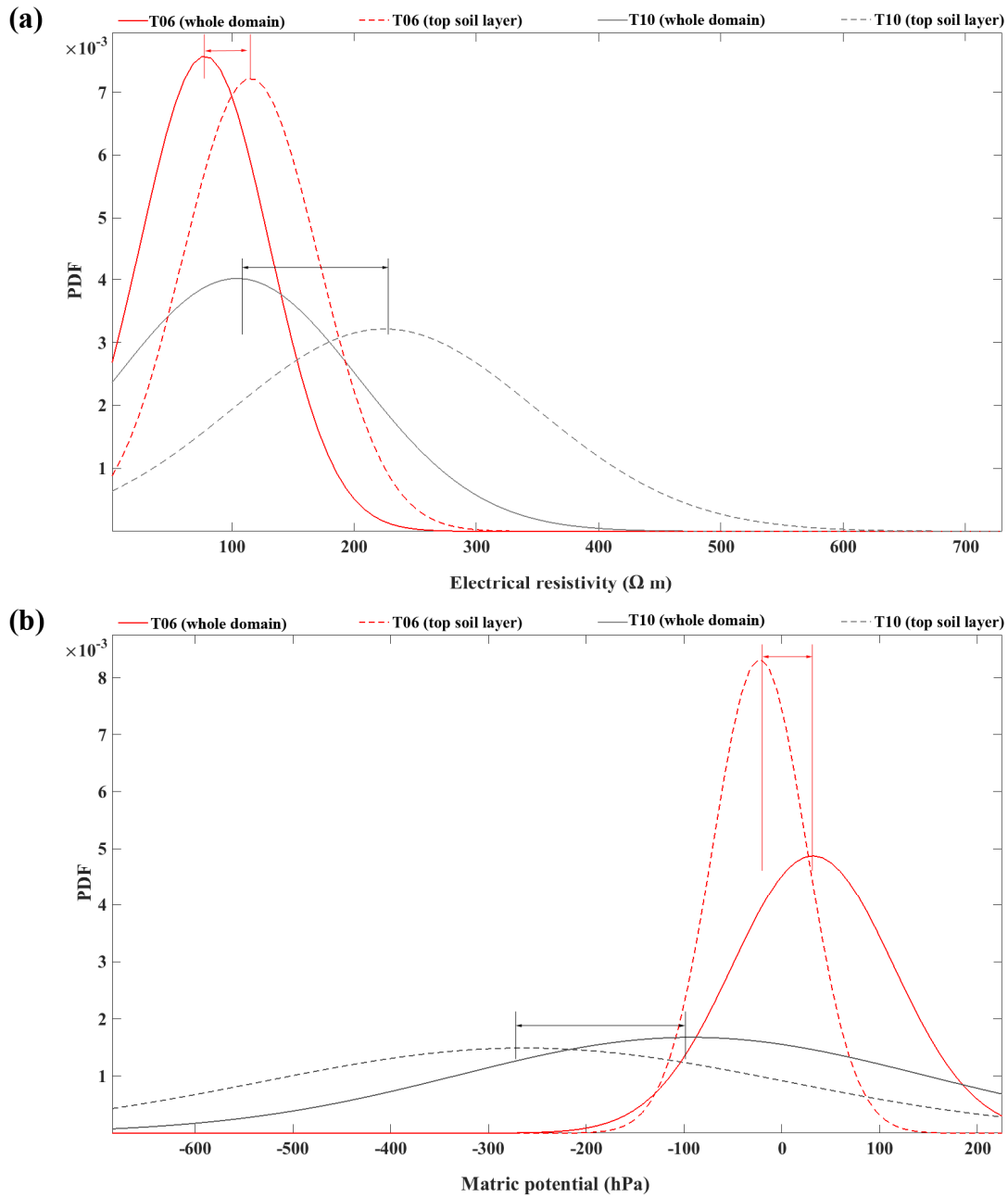
4  
5  
6  
7

Figure 4. ERT maps for the wettest (T06) and driest (T10) states. The 10 measurement dates (from T01 to T10) are in the supplements (Fig. S5). Black points indicate tensiometer locations and black arrow the hedgerow location.



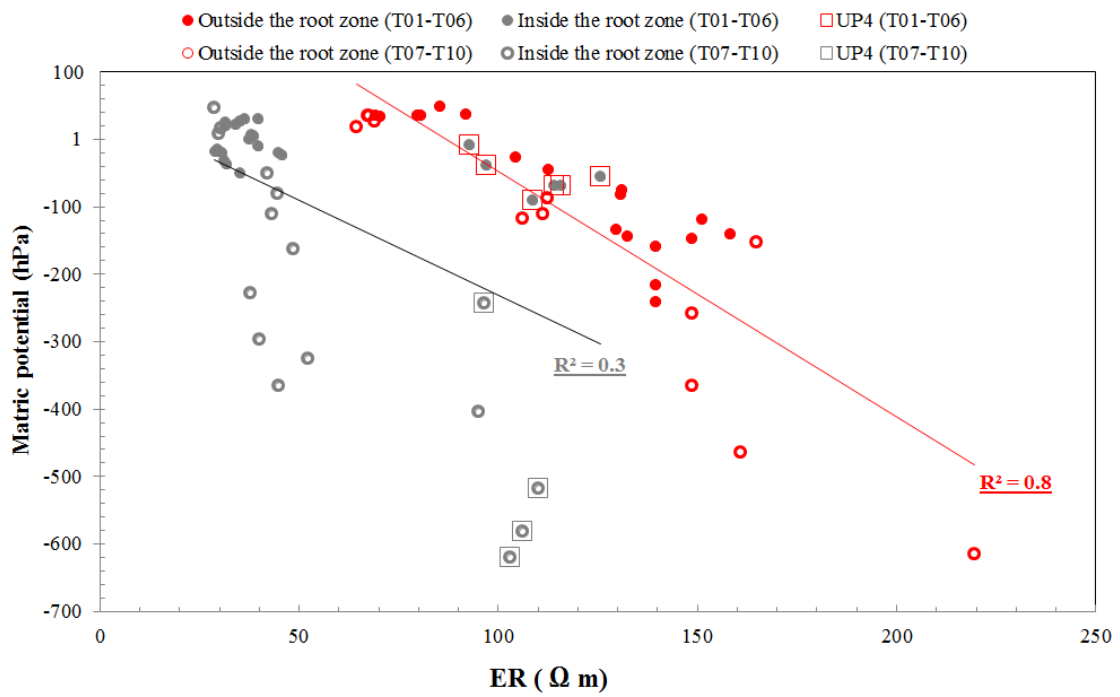
1  
 2 Figure 5. Relationship between ER and soil dryness at the hedgerow proximity. (a) Variation  
 3 (%) in electrical resistivity from the wettest state (T06) to the driest state (T10). (b) Measured  
 4 soil matric potential profiles at 7 locations: UP16, UP8, UP4 and UP1 for upslope and DW2,  
 5 DW6 and DW12 for downslope. Dashed lines indicate the wettest state (T06) and solid lines  
 6 the driest state (T10).





1

2 Figure 6. Probability density functions (Pdf) of (a) electrical resistivity and (b) matric  
 3 potential between wet (T06) and dry (T10) states for the entire domain (solid line) and the  
 4 topsoil layer (dashed line).



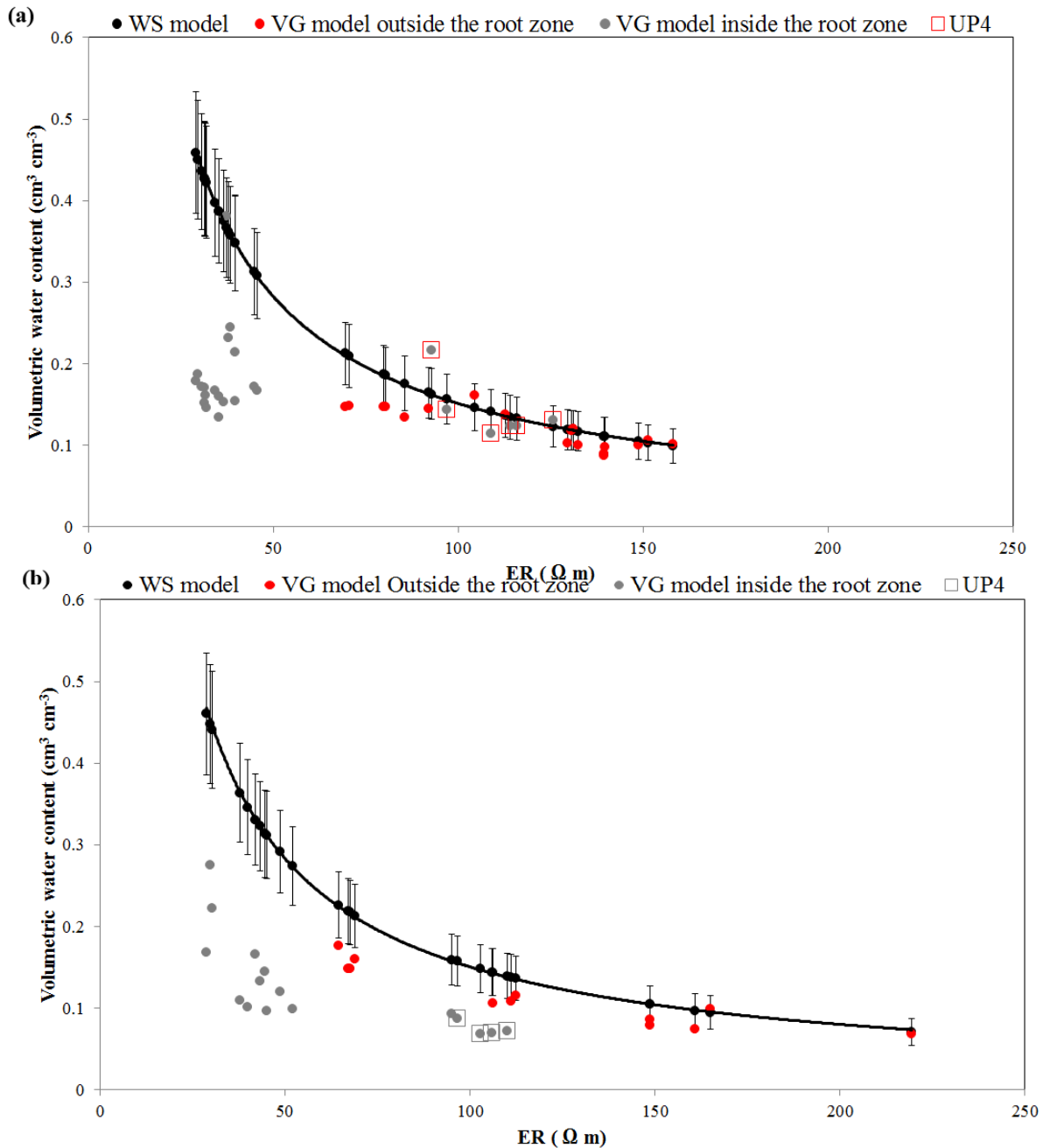
1

2 Figure 7. Relationship between matric potential and ER measured in the topsoil during the

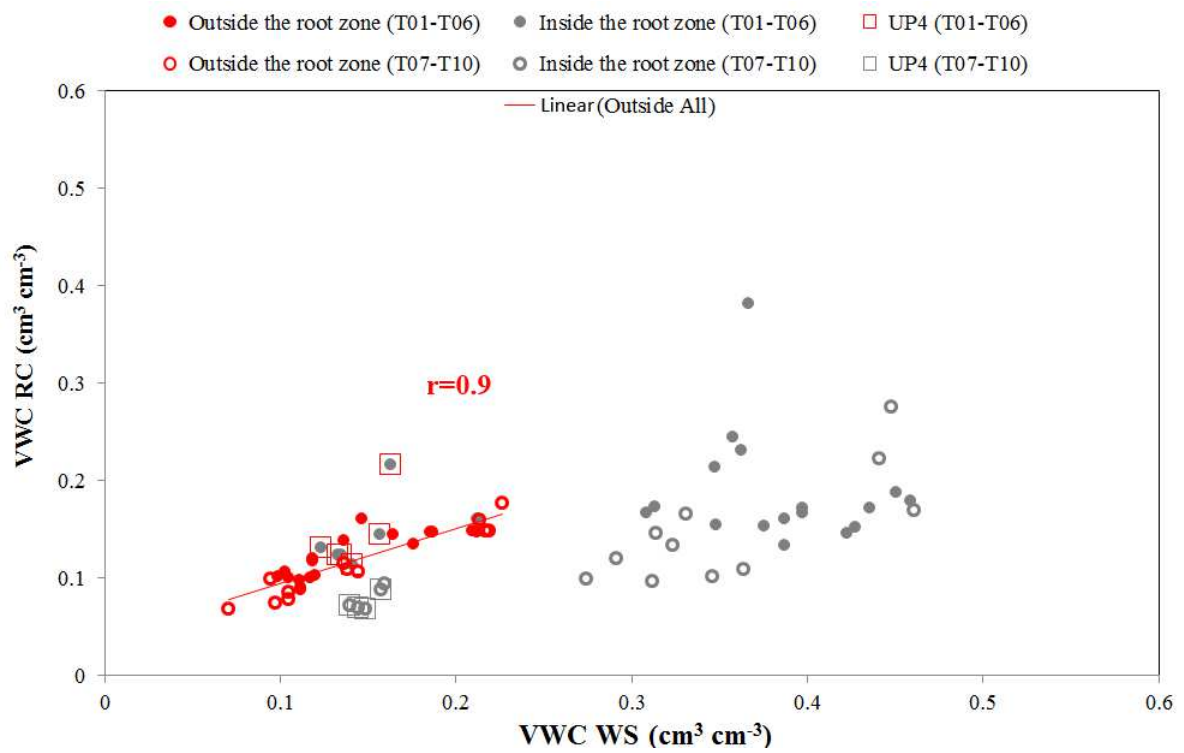
3 study period (T01-T10). Red and gray circles indicate the data collected regularly outside and

4 inside the root zone, respectively. Filled circles indicate the wet period (T01-T06) and open

5 circles the dry period (T07-T10).

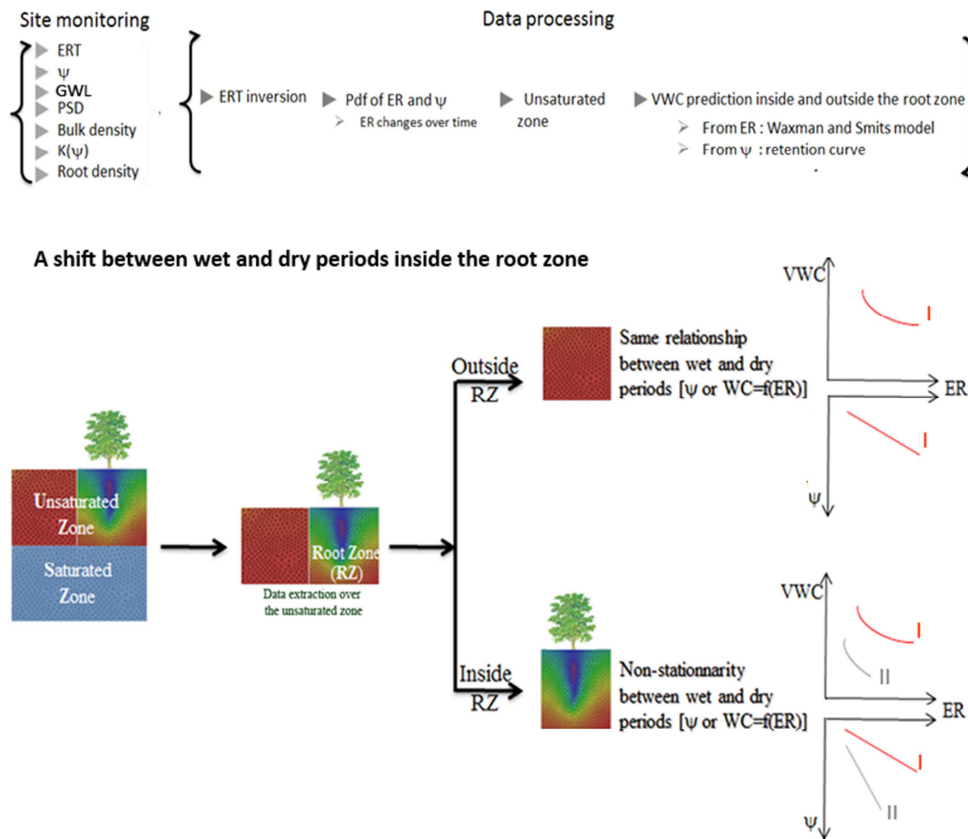


1  
 2 Figure 8. Relationship between VWC and ER in the topsoil for (a) the wet period (T01 to  
 3 T06) and (b) the dry period (T07 to T10). Black circles with standard deviation indicate VWC  
 4 from the Waxman and Smits model. Red and gray circles indicate VWC predicted from the  
 5 retention curve outside and inside the root zone, respectively.



1

2 Figure 9. VWC predicted by the Waxman and Smits model compared that predicted by the  
 3 retention curve outside the root zone (red circles) and inside the root zone (gray circles).  
 4 Filled circles represent the wet period (T01 to T06) and open circles the dry period (T07-  
 5 T10).



1  
 2 Figure 10. Conceptual diagram summarizing the monitoring setup and the main results,  
 3 Outside the root zone, the same relationships between ER and VWC (or matric potential)  
 4 were observed for the wet and dry periods (curve I). Two behaviors (curves I and II) were  
 5 observed on the locations inside and outside the root zone. .